PROCEEDINGS OF SCIENCE

Highlights from the Auger Engineering Radio Array

Bjarni Pont[a,*] **for the Pierre Auger Collaboration**[b,†]

[a] *Department of Astrophysics/IMAPP, Radboud University, P.O. Box 9010, NL-6500 GL Nijmegen, The Netherlands*

[b] *Observatorio Pierre Auger, Av. San Martín Norte 304, 5613 Malargüe, Argentina*

E-mail: spokespersons@auger.org

The Auger Engineering Radio Array (AERA) at the Pierre Auger Observatory is an array of 153 radio-antenna stations that measure the 30 − 80 MHz radio emission produced in extensive air showers in the energy range between 0.1 and 10 EeV. It has been taking data for over a decade. In this contribution, we present the recent results of AERA. We show the measurements of the depths of the shower maxima (X_{max}) using the radio footprint and using interferometry, demonstrating compatibility and competitiveness with the established fluorescence detection method. We also show the measurement of the stability of the radio signal over close to a decade determined using the Galactic radio background as a calibration source, demonstrating that a radio detector can be used to lower systematic uncertainties on the energy scale of, for example, fluorescence and water-Cherenkov detectors.

7th International Symposium on Ultra High Energy Cosmic Rays (UHECR2024)
17-21 November 2024
Malargüe, Mendoza, Argentina

*Speaker

†Full author list at https://www.auger.org/archive/authors_2024_11.html

 ISSN 1824-8039 . Published by SISSA Medialab.

PoS(UHECR2024)049

1. Introduction

Detecting *ultra-high-energy cosmic rays* (UHECRs) relies on the indirect observation of extensive air showers. These showers leave large-scale footprints on the ground, which can be captured by deploying arrays of detectors. By analyzing the collected data, the characteristics of the air showers can be reconstructed, providing insights into the nature and origin of cosmic rays. A crucial factor in distinguishing between different cosmic ray source models is the mass, or particle type, of the primary cosmic ray [1]. Although the mass cannot be directly measured, it can be inferred through observables such as the *depth of the shower maximum* (X_{max}). The altitude at which an air shower reaches its maximum development depends on the mass of the primary particle, i.e., showers initiated by heavier particles tend to develop higher in the atmosphere compared to those from lighter particles. Heavier particles behave like composites of multiple lighter particles, each carrying a portion of the total energy. As a result, the sub-showers initiated by these lower-energy particles conclude earlier, leading to a shallower X_{max} for heavier cosmic rays. Besides estimating the nuclear mass composition, the determination of cosmic ray energy is also required to understand its nature. For measurements spanning years or decades, it is important for this measurement to remain stable. Radio can act as a stable reference that does not significantly change over time, in principle providing a source of calibration for any other detector type. In this work, we present the recent results related to the energy and mass determination through radio signals emitted by air showers.

2. AERA and the Pierre Auger Observatory

The Pierre Auger Observatory [2], situated near Malargüe, Argentina, is designed to detect ultra-high-energy cosmic rays (UHECRs) at the most extreme energies. Spanning 3,000 km^2, it is the largest facility of its type globally. The primary infrastructure of the Observatory includes the *surface detector array* (SD), consisting of 1,660 *water-Cherenkov detectors* (WCD) with a recently added *scintillator surface detector* (SSD) and *radio detector* (RD) on top, along with the *fluorescence detector* (FD) positioned around and overlooking the SD. Additionally, the *Auger Engineering Radio Array* (AERA) [3], located in the western region of the SD, consists of a dense grid of radio antennas covering approximately 17 km^2. It has been measuring for the past decade and also functioned as the testbed for the recently installed RD. AERA captures radio signals generated by air showers within the frequency range of 30 to 80 MHz, and it is sensitive to events with energies exceeding about 10^{17} eV, extending up to 10^{19} eV-constrained by radio background noise at the lower end and by surface area and operational duration at the higher end. The combination of radio and various other detection techniques makes the Pierre Auger Observatory an ideal place to study both the properties of cosmic rays and the systematics of their detection techniques.

3. On Cosmic-Ray Energy

3.1 Radio as a stable calibration source

The energy of cosmic rays can be accessed with various detector types. Each method has its advantages and disadvantages. One of the causes of systematic uncertainty is the stability

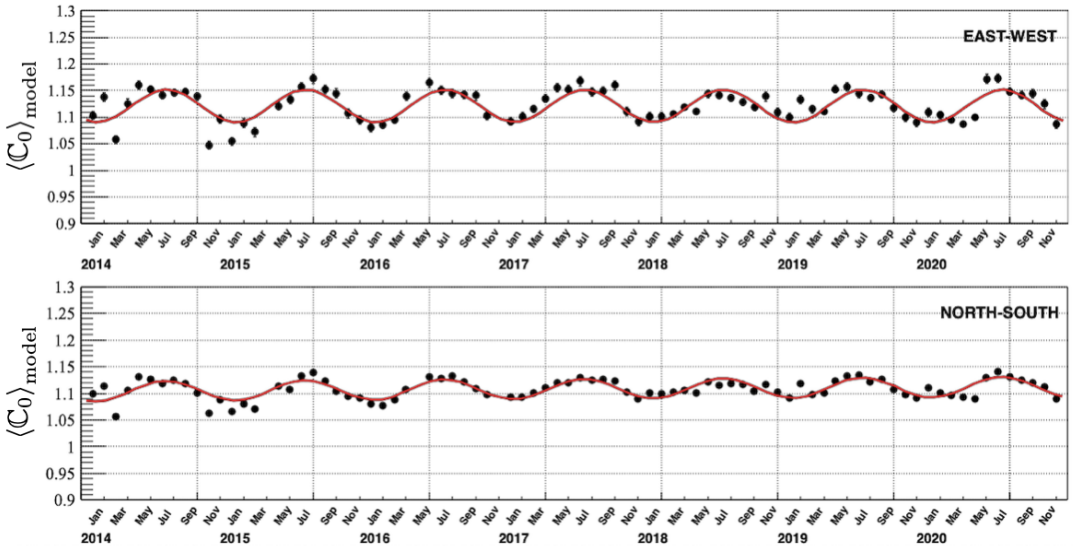

Figure 1: Average calibration constant per month for a single AERA station (black markers) for its east-west-aligned antenna (top) and north-south-aligned antenna (bottom). A cosine fit with an additional linear slope parameter is fitted (red line).

of the measurement over time. For example, dust accumulation on the mirrors of fluorescence telescopes affects the amount of measured light and the photomultiplier tubes used in both WCD and fluorescence detectors are known to decrease in efficiency over time. Both affect the estimation of the cosmic-ray energy. These ageing effects can be accounted for to an extent but some level of systematic uncertainty currently remains [4]. To reduce this systematic, we would need a new 'standard candle' to which we can calibrate the energy scale. Radio can provide this because it continuously measures the background radio emission from the Milky Way.

Models of the radio sky made with sky surveys from various radio telescopes around the world provide the estimated power in the AERA antennas, and by comparing this to the measured radio background, we can track the sensitivity of the radio antennas over time. In Figure 1 we show the results of this measurement for a single AERA station. In both panels, the average calibration constant $\langle \mathbb{C}_0 \rangle$, which is the square root of the ratio of the measured versus expected Galactic power, averaged over the AERA frequency band for each month, is plotted. More details can be found in [5]. The measurements span a period of 7 years, showing no evolution over that period (besides a likely seasonal variation represented by an added cosine to the otherwise linear fit). The slope is calculated for each antenna of AERA, and after accounting for method and sky model uncertainties, we obtain a constraint on the ageing of the radio cosmic-ray energy of $0.32 \pm 0.51\%$ per decade. This shows that there is no significant ageing such that measurements of cosmic-ray energy done by radio can be a standard candle for other detector types measuring the energy. So, by comparing the cosmic-ray energy measured simultaneously by both radio [6] and measured by the SD or FD, we can establish the ageing effects independently from manual in-situ measurements, allowing us to increase the reliability of such corrections and potentially reduce systematic uncertainties overall.

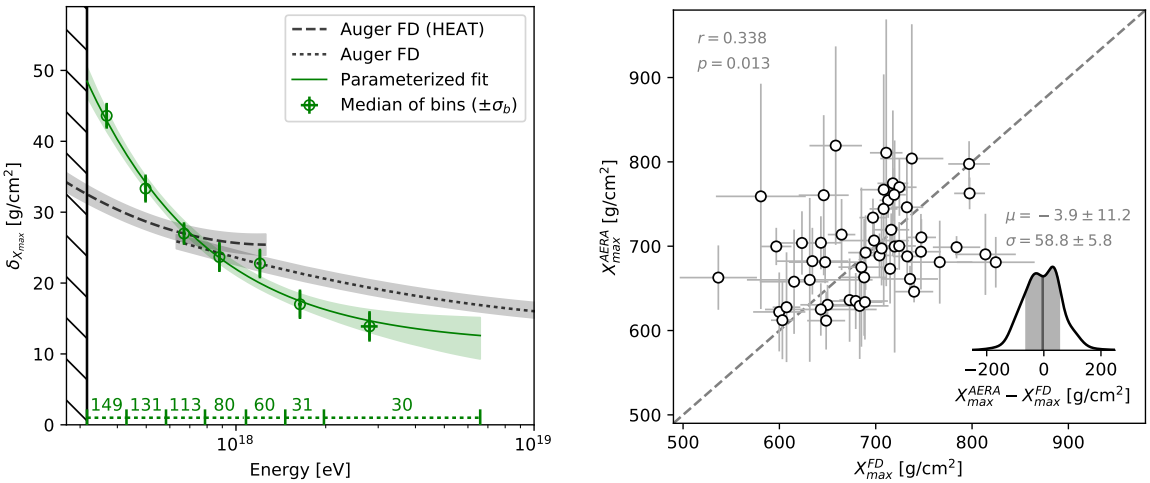

Figure 2: Left: Median resolution of the $X_{\max}$ reconstruction for 7 energy bins, as marked at the bottom of the figure. Annotated are the number of events per bin. A parameterized fit to the medians of the bins is shown. The $X_{\max}$ resolution for the FD is shown in black. The hatched region marks the region excluded by quality cuts. **Right**: Comparison of $X_{\max}$ reconstructed with both AERA and the FD. Annotated are the Pearson correlation coefficient r and its p-value, and the mean and spread of the difference of the two methods. A kernel density of this density is shown in the inset in the bottom right. A diagonal line has been added to guide the eye.

4. On Cosmic-Ray Mass Composition

There are two main observables used to access the mass composition information using the radio emission. The first is the electron-to-muon ratio, where one combines the muon content estimation from the WCD [7] and the electromagnetic energy from radio. Recent results of this method are shown in [8]. The second mass-sensitive observable is the depth of shower maximum $X_{\max}$. The radio footprint on the ground changes its shape depending on the distance to the shower maximum. For showers coming from above (and in this work up a zenith angle of 55°) this gives access to high-quality $X_{\max}$ measurements as will be described below. For higher zenith angles the sensitivity to the mass rapidly drops because the shower maximum will be very far away for any particle mass, decreasing the separation power. Luckily, using interferometry, this measurement can be done with much higher precision such that it is still viable to extract a high-resolution $X_{\max}$. The higher precision requirement is aided significantly by the large radio footprints for inclined showers, resulting in a large number of antennas to perform the interferometry. This second method will also be described in more detail below.

4.1 $X_{\max}$ from the radio footprint

The radio footprint on the ground changes with $X_{\max}$ of the shower due to where the emission is generated. By creating a set of air shower simulations with varying $X_{\max}$ for a measured event, one can try to match this to the observed radio footprint in order to extract $X_{\max}$. We performed high-detail air-shower simulations, including the effects of a time-dependent magnetic field, the GDAS atmospheric density and refractive index profiles, and the background noise recorded with AERA to accurately match the measurement conditions. Next, a likelihood approach is used to

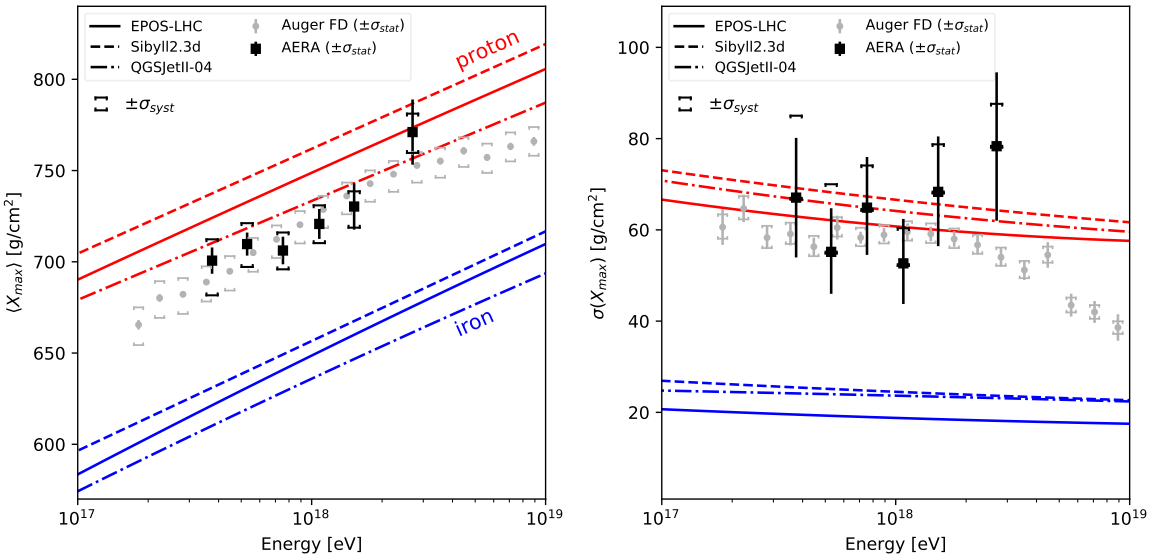

Figure 3: First two moments of the $X_{\max}$ distribution as measured by AERA as a function of SD-measured cosmic-ray energy. Model lines for proton and iron nuclei are added for comparison. Also, the FD-measured moments are shown for comparison. The vertical bars indicate statistical uncertainties and the capped markers show the systematic uncertainties.

match the simulations to the measured shower, evaluating and correcting for reconstruction biases and determining the reconstruction uncertainty. The method is described in detail in [9–11]. We compare the results to measurements of the FD on an event-by-event basis and find no significant bias and a spread of the measurements compatible with the combined resolutions of the two detectors (see Figure 2, left). Furthermore, we find that the $X_{\max}$ resolution is in the same order as for the FD (see Figure 2, right). In Figure 3 we show the two moments of the $X_{\max}$ distribution of the full AERA $X_{\max}$ dataset. Also, the results of the full dataset are compatible with the FD measurements. In Figure 4 we show the distribution of AERA $X_{\max}$ measurements compared to the FD-measured composition when including the detector effects of AERA (acceptance, resolution, and reconstruction bias). An Anderson-Darling test is done, and for each of the 6 energy bins, compatibility is obtained. These results show that $X_{\max}$ is both compatible and competitive with the established fluorescence method.

4.2 $X_{\max}$ from radio interferometry

To extend the sensitivity of $X_{\max}$ to higher zenith angles, where the shower maximum is very far away, radio interferometry [12] can provide the required extra sensitivity. By coherently summing the signals from the radio stations, we reduce the background noise significantly. The location of the emission region is found by calculating the time delay for each antenna for each position and evaluating the coherent sum of all the signals. Also, for this method, the GDAS atmospheric model is used to account for the effects of the refractive index on the propagation time. Crucial for this method is the time synchronization of the antennas, which should be in the order of a nanosecond. This is done with an AERA beacon signal deployed near AERA [13].

From the 3D map of coherent emission that is obtained, we can extract the shower axis by

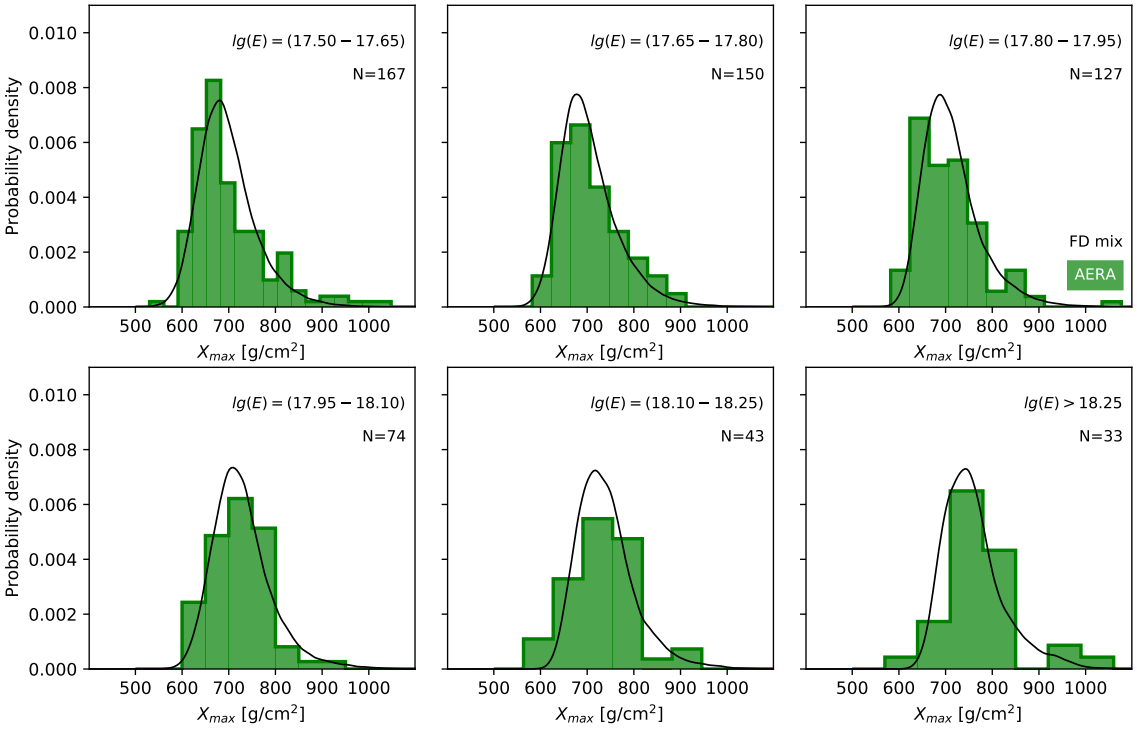

Figure 4: Distribution of the measured $X_{\max}$ values in 6 energy bins. Annotated are the energy ranges and the number of events in each bin. The black curves show the expected $X_{\max}$ distribution when forward-folding the FD-measured composition through the efficiency, resolution, and reconstruction bias of the AERA detector, allowing for direct comparison (see the main text).

fitting the region of the highest signal. This map also provides a profile of the emission along the shower axis. The depth of radio interferometric maximum, $X_{\rm rit}$, can be related to $X_{\rm rit}$ obtained for the set of simulated showers in the same way as was done for the footprint method. In the left panel of Figure 5 we show an example of $X_{\rm rit}$ vs $X_{\max}$ for the simulations performed for a single measured event. The linear relation between $X_{\rm rit}$ and $X_{\max}$ (red line) is used to relate the $X_{\rm rit}$ value of the measured shower (blue line with uncertainty) to the $X_{\max}$ value that the measured shower should have. For comparison, the $X_{\max}$ value obtained with the footprint method is shown too (yellow line). A good agreement is obtained between $X_{\max}$ from the two methods showing a rather deep shower. To highlight the performance in various conditions, the comparison of the two methods is also shown for a shallow shower of about 600 g cm^{-2} (middle panel) and a lower quality measurement of a shower with fewer stations (right panel). Both provide compatible reconstructions of $X_{\max}$ between the interferometric and footprint methods. Note that the estimation of uncertainty of the interferometric method is currently a work in progress.

These examples demonstrate the viability of the method to reconstruct $X_{\max}$ with interferometry. This is particularly interesting for the recently deployed AugerPrime Radio Detector [14] that added 1660 radio antennas, one to each of the existing WCDs. With a new beacon system currently under development for the RD, interferometry can become a viable method for obtaining mass composition in addition to the electron-muon separation.

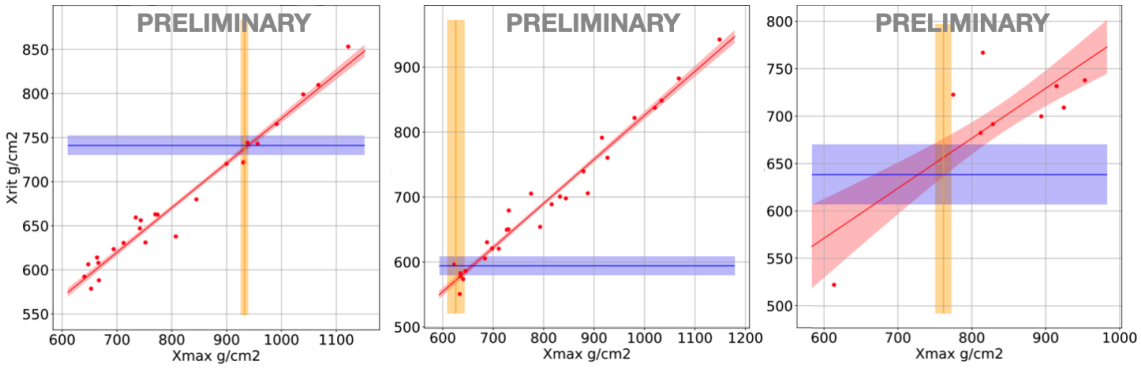

Figure 5: Three examples of reconstructed X_{rit} of a measured shower (blue line), a set of simulated showers representing the measured shower with a range of X_{max} possibilities (red points with linear fit). The intersect provides an estimation of X_{max} of the measured shower. For comparison, the X_{max} values of these events with the footprint method is shown (yellow lines).

5. Conclusions

We have presented the recent results of the Auger Engineering Radio Array, highlighting its contributions to the measurement of cosmic-ray energy and mass composition. The stability of radio signal in AERA over nearly a decade demonstrates its potential as a calibration standard, potentially reducing the systematic uncertainties in energy scale in the future. Furthermore, we showed that X_{max} measurements from the footprint method are competitive and compatible with the established fluorescence technique. The preliminary results from the interferometric method show promising agreement and might extend the mass sensitivity to higher shower inclinations in the future. These results highlight the value of radio detection as a complementary tool to measure and understand ultra-high-energy cosmic rays and demonstrate how these methods can be applied on a larger scale at, for example, the AugerPrime Radio Detector.

References

[1] A. Abdul Halim *et al.* (Pierre Auger Collaboration), *J. Cosmol. Astropart. P.* **05** (2023) 024

[2] A. Aab *et al.* (Pierre Auger Collaboration), *Nucl. Instrum. Meth. A* **798** (2015) 172–213

[3] P. Abreu *et al.* (Pierre Auger Collaboration), *J. Instrum.* **7** (2012) P10011

[4] B. Dawson [for the Pierre Auger Collaboration], PoS(ICRC2019)231

[5] D. Correia dos Santos [for the Pierre Auger Collaboration], PoS(ICRC2024)030

[6] A. Aab *et al.* (Pierre Auger Collaboration), Phys. Rev. Lett. **116**, 241101 (2016).

[7] A. Aab *et al.* (Pierre Auger Collaboration), Phys. Rev. D. **91**, 059901 (2015).

[8] M. Gottowik [for the Pierre Auger Collaboration], PoS(ARENA2024)033

[9] A. Abdul Halim *et al.* (Pierre Auger Collaboration), Phys. Rev. Lett. **132**, 021001 (2024).

[10] A. Abdul Halim *et al.* (Pierre Auger Collaboration), Phys. Rev. D. **109**, 022002 (2024).

[11] B. Pont, Ph.D. thesis, Radboud University, 2021.

[12] H. Schoorlemmer [for the Pierre Auger Collaboration], PoS(ICRC2023)380

[13] F. G. Schröder *et al.*, Nucl. Instr. Meth. A **615**, 277–284 (2010).

[14] J. Pawlowsky [for the Pierre Auger Collaboration], PoS(ICRC2023)344